Multiconductor Cell Analysis of AC High Speed Railway Lines

Roberto Benato, *Senior Member, IEEE*, Giovanni Gardan, *Member, IEEE*, and Luca Rusalen, *Member, IEEE*

***Abstract*— The aim of this article is the application of Multiconductor Cell Analysis (MCA) to a very special case of a multiconductor system, i.e., the AC high-speed railway system, with 14 parallel conductors. The present matrix approach allows representing both the single elements and the entire railway system also including the high-voltage (HV) three-phase supply network. The algorithm allows computing all the steady-state regime electrical quantities (voltages, currents, and power) of each section: in particular, the ground return current, responsible for electromagnetic interferences (EMIs), can be derived by the knowledge of all the circulating currents. It is also possible to evaluate the electric unbalance impact on the supply three-phase power system given by the railway system. Eventually, two different scenarios are presented, i.e., a maximum allowable high-speed line power request and a contact-wire-to-rail short circuit.**

***Index Terms*— High speed railway lines, multiconductor transmission lines, power quality, power system analysis.**

I. Introduction

A. Motivation

CLIMATE change and environmental degradation are an existential threat to Europe and the world. Nowadays, the transport sector contributes to about 25% of the EU's total greenhouse gas emissions and this value has increased over recent years. In the European Green Deal, a set of proposals is presented to make Europe the first climate-neutral continent by 2050. This requires ambitious changes in transport in order to reduce greenhouse gas emissions by 90% by 2050 in the transport sector [1]. Passenger traffic on the high-speed rail will double by 2030 compared to 2020 [2]. Railways have a high energy efficiency for several reasons, the chief ones are the very low rolling resistance of wheels on track, the high efficiency of the traction chain, and their large carrying capacity of both passengers and freight. On average, rail is nearly 12 times more energy efficient than cars per passenger per kilometer and 11 times more than aviation. For freight transport, trains are 6 times more energy efficiency than trucks [3]. In this frame of reference, the rail sector will play a key role in containing greenhouse gases emissions. The electrical regime evaluation of the AC high speed railways lines has its roots in the 1980s by means of the large-scale diffusion of this kind of power supply system. Different papers have been presented over the years in order to analyze different aspects, e.g., [4], [5], [6], [7], [8], [9], [10], [11], [12], [13], [14], some of these allow computing electrical quantities along a section of the traction systems [4], [5], [6], [7], [8], [9], [10], [11], [12], instead, other papers focus on the harmonic behavior [13], [14]. Unluckily, some researches exploit a simplified traction system configuration [4], [5], [7], [11], [12], whereas, no paper allows studying the electrical regime of an entire AC high-speed line, by considering all the system elements, both the HV supply system and the catenary. The knowledge of the entire railway steady-state regime, by analyzing also the detailed electrical behavior along the track, allows one to ensure the correct operation of the system elements. A detailed electrical assessment of the AC railway supply system is fundamental in order to evaluate its insertion into the AC electric grid in terms of power quality, e.g., unbalance factor containment. Furthermore, the matrix approach presented in this article is an open algorithm that can be easily self-implemented and it allows for studying the regime of every AC high-speed railway line present today.

B. Literature Review

The multiconductor cell analysis (known in technical literature with its acronym MCA) is a matrix-based open algorithm first published in 2009 by the first author. It allows studying the steady-state regime of asymmetrical power systems in a phase frame of reference, without simplifying hypotheses (e.g., resorting to sequence frame of reference) and without neglecting passive conductors (e.g., earth wires of overhead lines, metallic screens/armors of land/submarine cables).

MCA has been successfully applied to a great number of asymmetrical systems as follows.

1) Distribution line carriers [15].
2) Milliken-type cables [16].
3) Three-core submarines cables [17].
4) Land cables protected by steel reinforced concrete structures [18], [19].

It is worth noting that MCA is one of the rare example of an algorithm which has had two experimental validations by means of the following.

1) Capri-Torre Annunziata 30 km long three-core armored submarine cable (validation only at 50 Hz) [20].
2) Malta-Sicily 100 km long three-core armored submarine cable (validation at harmonic frequencies up to 40th harmonic order) [21].

Manuscript received 2 December 2022; revised 23 January 2023; accepted 7 February 2023. Date of publication 13 February 2023; date of current version 13 September 2023. *(Corresponding author: Roberto Benato.)*

The authors are with the Department of Industrial Engineering, University of Padua, 35131 Padua, Italy (e-mail: roberto.benato@unipd.it; giovanni.gardan@phd.unipd.it; luca.rusalen@phd.unipd.it).

Digital Object Identifier 10.1109/TTE.2023.3244272

In this article, MCA is applied to AC high-speed railway supply system which is an asymmetrical power system due to the following.

1) 14 metallic conductors: the active ones, i.e., contact wires, the messengers, the feeders, and the passive ones, i.e., the return wires, the buried ground wires, and the rails.
2) The resulting multiconductor system is supplied, for subsequent sections, by three-winding transformers, which induce on the high-voltage (HV) transmission grid unbalanced power absorption.

There are also two other contributions which deserve to be mentioned [22], [23].

The first paper [22] has a different approach of MCA: in fact, in order to obtain the PI-circuit of a multiconductor system, it is possible (differently from MCA) to generalize the PI-circuit of single-phase circuit by means of the modal analysis. This involves the evaluation of hyperbolic functions of the matrix of the propagation constant. Since there is no direct way of computing the sinh or tanh of a matrix, it is necessary to use the modal analysis, which allows solving this calculation by means of eigenvalues and eigenvectors. As demonstrated in [15], the comparison between MCA and the modal analysis is fully satisfactory and shows that there are some drawbacks with the modal analysis due to not particularly accurate calculations of eigenvalues and eigenvectors by using the native functions of MATLAB. In fact, the modal analysis needs a very accurate determination of eigenvalues and eigenvectors (in technical literature, it is suggested the use of Wilkinson and Reinsch with due regard). Moreover, in [22], there are no numeric results.

The second paper [23] deals with the harmonic analysis and it is not an open algorithm but it uses a closed software: in fact, the harmonic analysis model is developed by the PSCAD/EMTDC (power systems computer-aided design/electromagnetic transients including DC) program. This approach is diametrically opposite to MCA. Moreover, the article considers an eight-port representation, i.e., two contact lines, two feeders, and four rails, whereas the present approach considers a 14-port representation (i.e., all the present conductors), which allows computing the ground return current differently from [23] which cannot compute it.

C. Contribution

In this article, the high-speed railway power supply 2×25 kV is modeled thoroughly without simplifying hypotheses and without neglecting any active or passive conductor. MCA allows knowing the circulating currents in the active conductors and the induced currents in the passive ones. Moreover, this knowledge allows computing the ground return current along the entire railway path. Therefore, the electromagnetic interferences (EMIs) and the possible AC corrosion effects can be assessed by means of the results of this article.

Firstly it is presented how the different system elements are modeled. Therefore, two different practical scenarios are studied to confirm the validity of the method; in the former the contemporary presence of 16 trains along the track is considered, in the latter a fault in a generic k position is analyzed. In both cases, the electrical quantity behavior along the path is computed, in order to have a safe traction system operation.

II. MCA Method Fundamentals

A. Multiconductor System Elementary Cell

A n conductors system parallel to themselves and to the ground can be considered as a cascade of elementary cells of length Δ (see Fig. 1). Being Δ sufficiently small, it is possible to lump distributed shunt admittances at the end sections of the cell s and r, this allows separating the study of longitudinal elements from the transversal ones. In matrix relations of Fig. 1 the column vectors $\underline{\boldsymbol{u}}_s$ and $\underline{\boldsymbol{u}}_r$ represent the voltage at the two cell ends, whereas the vectors $\underline{\boldsymbol{i}}_s$, $\underline{\boldsymbol{i}}_r$, $\underline{\boldsymbol{i}}_{sL}$, $\underline{\boldsymbol{i}}_{sT}$, $\underline{\boldsymbol{i}}_{rL}$, $\underline{\boldsymbol{i}}_{rT}$ represent the entering currents into the elements. The admittance matrix $\underline{\boldsymbol{Y}}_T$ $(2n \times 2n)$ allows considering the behavior of the transversal elements; this matrix can be computed starting from the admittance matrices $\underline{\boldsymbol{Y}}_{ssT}$, $\underline{\boldsymbol{Y}}_{ssT}$ $(n \times n)$ of each transversal block T, i.e.,

$$\underline{\boldsymbol{Y}}_T = \left[\begin{array}{c|c} \underline{\boldsymbol{Y}}_{ssT} & \\ \hline & \underline{\boldsymbol{Y}}_{rrT} \end{array}\right].$$

These two matrices can be easily computed if the distributed susceptances on $\Delta/2$ are lumped at each ends. The capacitive susceptances (of half cell) between each conductor are considered in each block matrix. For the evaluation of $\underline{\boldsymbol{Y}}_L$, the Carson theory is exploited; this approach allows determining the self and mutual longitudinal impedances (if $d \gg \Delta$ is assumed, with d equal to the line length, the border effects can be neglected) considering also the electromagnetic field inside the earth.

It has been widely demonstrated by Benato et al. [24] that at power frequency (50 or 60 Hz) the Carson-Clem formulae are very precise and consequently they are a powerful tool so giving the same results of complete Carson ones. In order to give the above-mentioned sentence a theoretical justification, the simplified Carson-Clem formulae can be licitly applied if the spacing between conductors $d_{i,k} \leq 0.135 D_e$ when $D_e = 658 \cdot \sqrt{\rho/f}$ m "Carson Depth"; ρ = electrical resistivity of the soil (Ωm); f = power frequency (50–60 Hz). By supposing $f = 50$ Hz and a low earth resistivity, e.g., 10 Ωm, it yields $D_e = 294$ m. So, the spacings between conductors in high speed railway line are never greater than 15 m, therefore it is rather unlikely to have the condition $d_{i,k} \geq 0.135 D_e \cong 40$ m even with very low resistive earth; hence the Carson-Clem formulae can be always used. The self and mutual impedances by means of Carson-Clem formulae are given by

$$\underline{z}_{i,i} = r_i + \pi^2 \cdot 10^{-4} \cdot f + j4\pi \cdot 10^{-4} \cdot \ln\left(\frac{2 \cdot D_e}{d'_i}\right) \quad (1)$$

$$\underline{z}_{i,k} = \pi^2 \cdot 10^{-4} \cdot f + j4\pi \cdot 10^{-4} \cdot \ln\left(\frac{D_e}{d_{i,k}}\right) \quad (2)$$

where r_i = kilometric resistance of conductor i (Ω/km); $d'_i = 2 \cdot \mathrm{GMR} = k'' d$ (m) (GMR = geometrical mean radius) where k'' are listed in tables depending upon the composition of the

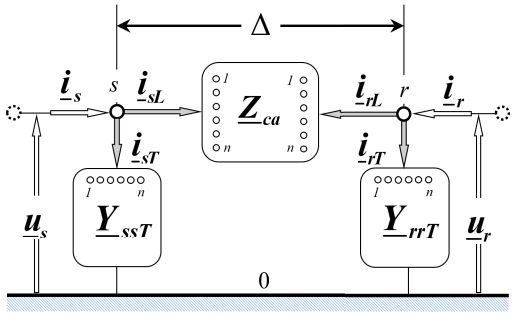

Fig. 1. Traction line elementary cell.

conductor and d (m) is the diameter of the conductor; $d_{i,k}$ = distance between conductor i and k (m).

In this way, the matrix $\underline{\boldsymbol{Z}}_{ca}$ ($n \times n$) can be computed. This matrix appears (by considering $\underline{\boldsymbol{i}}_{\mathbf{rL}} = -\underline{\boldsymbol{i}}_{\mathbf{sL}}$) in the following formulations:

$$\underline{\boldsymbol{u}}_s - \underline{\boldsymbol{u}}_r = \underline{\boldsymbol{Z}}_{ca}\underline{\boldsymbol{i}}_{sL} \tag{3}$$

$$\underline{\boldsymbol{u}}_s - \underline{\boldsymbol{u}}_r = -\underline{\boldsymbol{Z}}_{ca}\underline{\boldsymbol{i}}_{rL} \tag{4}$$

being $\underline{\boldsymbol{Z}}_{ca}$ not singular, it yields

$$\underline{\boldsymbol{i}}_{sL} = \underline{\boldsymbol{Z}}_{ca}^{-1}(\underline{\boldsymbol{u}}_s - \underline{\boldsymbol{u}}_r) \tag{5}$$

$$\underline{\boldsymbol{i}}_{rL} = -\underline{\boldsymbol{Z}}_{ca}^{-1}(\underline{\boldsymbol{u}}_s - \underline{\boldsymbol{u}}_r). \tag{6}$$

These two equations can be written in compact matrix form

$$\begin{bmatrix} \underline{\boldsymbol{i}}_{sL} \\ \underline{\boldsymbol{i}}_{rL} \end{bmatrix} = \left[\begin{array}{c|c} \underline{\boldsymbol{Z}}_{ca}^{-1} & -\underline{\boldsymbol{Z}}_{ca}^{-1} \\ \hline -\underline{\boldsymbol{Z}}_{ca}^{-1} & \underline{\boldsymbol{Z}}_{ca}^{-1} \end{array}\right] \begin{bmatrix} \underline{\boldsymbol{u}}_s \\ \underline{\boldsymbol{u}}_r \end{bmatrix}. \tag{7}$$

The following relation is obtained:

$$\underline{\boldsymbol{i}}_L = \underline{\boldsymbol{Y}}_L \underline{\boldsymbol{u}}. \tag{8}$$

The knowledge of $\underline{\boldsymbol{Y}}_L$ and $\underline{\boldsymbol{Y}}_T$ allows computing the admittance matrix $\underline{\boldsymbol{Y}}_C$ of the elementary cell

$$\underline{\boldsymbol{Y}}_C = \underline{\boldsymbol{Y}}_T + \underline{\boldsymbol{Y}}_L.$$

It is important to highlight that in real installations the magnitudes of $\underline{\boldsymbol{i}}_{sT}$ and $\underline{\boldsymbol{i}}_{rT}$ are lower than $\underline{\boldsymbol{i}}_s$ and $\underline{\boldsymbol{i}}_r$, so the induced border effects can be neglected. Furthermore, it could be interesting to note that the present method exploits the π-circuit, as represented in Fig. 1. This representation has a close conceptual analogy with the one used for an equivalent single-circuit at the positive sequence. The real configuration of the multiconductor high-speed railway involves 14 conductors: Fig. 2 shows the arrangement and the nomenclature of the multiconductor system. Consequently, the dimension of the elementary cell admittance matrix $\underline{\boldsymbol{Y}}_C$ is 28 × 28. The cell length Δ is assumed equal to 62.5 m, equivalent to a typical span length of the traction lines.

B. Cascade Composition of the Elementary Cells

Once the elementary cell admittance matrix is obtained, it is useful to consider the cascade of 12 cells: it is possible to calculate the admittance matrix of a 750 m subsection. The procedure to compute the cell cascade (28 × 28) is throughout reported in [25].

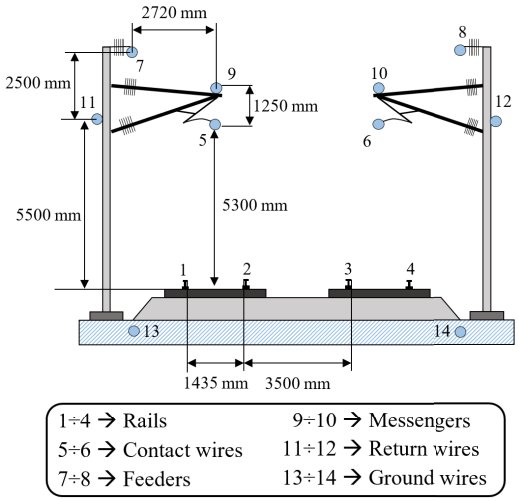

Fig. 2. Geometrical cross section of the high-speed railway system.

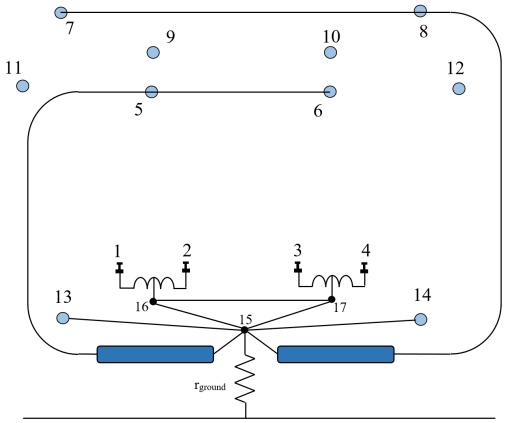

Fig. 3. Circuit model of the autotransformer installed along the railway line.

C. Shunt Elements

In order to complete the system representation, it is fundamental to include also the matrices modeling the shunt elements in some rail positions. These matrices can take into account the presence of autotransformers, line traps, earth connections, the loads representing the trains, or the possible short-circuits between the conductors. The admittance matrix $\underline{\boldsymbol{Y}}_S$ (14 × 14) of each shunt element can be computed by means of a primitive matrix $\underline{\boldsymbol{Y}}_P$ and an incident matrix $\boldsymbol{R}$ [26], [27].

A fundamental power system element is the autotransformer installed every 12 km along the railway line in a dedicated substation. The autotransformer rated power is equal to 15 MVA and has a very low short circuit voltage (e.g., 1%). The admittance matrix $\underline{\boldsymbol{Y}}_S$ is derived by the use of primitive matrix, which must also include the presence of mutual couplings. Fig. 3 shows a typical autotransformer installation where the line traps and the substation earthing grid are also present. In order to consider all the elements, it is necessary to add three additional nodes (in Fig. 3 represented by the nodes: 15–17) which must be removed by means of Kron's matrix reduction technique [28].

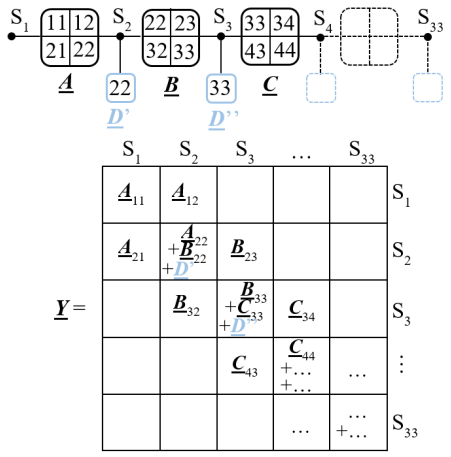

Fig. 4. Section matrix composition by means of subsection and shunt matrices.

D. Section Matrix Assembly

The typical 24 km section is composed by 32 750 m subsections. Once all the subsection matrices $\underline{\boldsymbol{A}}$, $\underline{\boldsymbol{B}}$, $\underline{\boldsymbol{C}}$, . . ., and the shunt element matrices $\underline{\boldsymbol{D}}$', $\underline{\boldsymbol{D}}$'',. . ., are computed, it is possible to combine the section matrices as shown in Fig. 4 with obvious matrix nomenclature. The section admittance matrix $\underline{\boldsymbol{Y}}$ with dimensions 462 × 462 ($n \cdot N \times n \cdot N$ with the number of subsection ends $N = 33$) is a diagonal block matrix. Each section can include subsections with different configurations due to the different situations: plains, tunnel, overpass, bridge, the train position, the train power absorption ($\underline{\boldsymbol{D}}_{\text{train}}$) or the fault presence ($\underline{\boldsymbol{D}}_{\text{fault}}$).

III. Line Matrix

A. Partial Separation Matrix

As represented in Fig. 5, at both the section ends, the contact wires 5 and 6, the corresponding messenger wires 9 and 10, as well as the feeders 7 and 8 present a separation point. Instead, the rails, the return wires and the buried ground wires have not got separation points. The longitudinal discontinuity can be easily represented by means of a specific matrix. This matrix inglobes only longitudinal links; the value of the matrix elements depends on the link typology: for the open conductors a great resistance value is imposed, instead, a small value is adopted for the not interrupted conductors. The separation conductance matrix $\underline{\boldsymbol{Y}}_{\text{sep}}$ is easily computed by inversion.

B. Section Matrix Reduction and Line Matrix Assembly

To analyze the matrix representation of the entire 192 km high-speed rail track, the cascade of eight sections, with the corresponding partial separation cells, must be considered. It should be kept in mind that the subsection composition creates an admittance matrix $\underline{\boldsymbol{Y}}$ with great dimensions. This matrix could be prohibitive for a standard workstation. However, it is firstly possible to characterize each section through a reduced matrix (but not simplified) $\underline{\boldsymbol{Y}}(1^{\text{st}}) \div \underline{\boldsymbol{Y}}(8^{\text{th}})$ (28 × 28). These matrices summarize the section behavior as seen at the ends. The global matrix $\underline{\boldsymbol{Y}}_{\text{glob}}$ (224 × 224) represents the complete high speed track behavior by considering also the partial separation matrix (as represented in Fig. 6). This matrix characterizes the passive high speed track system as seen at the 16 section ends (each one with 14 conductors).

IV. Regime of the Entire High Speed System

For the high speed track as seen at the 16 section ends, the following equation can be written:

$$\underline{\boldsymbol{u}}_S = \underline{\boldsymbol{Z}}_{\text{glob}} \underline{\boldsymbol{i}}_S \tag{9}$$

where $\underline{\boldsymbol{u}}_S = [\underline{\boldsymbol{u}}_1, \ldots, \underline{\boldsymbol{u}}_{16}]^T$ is the (224 × 1) block vector of all the section voltages (see Fig. 6) and $\underline{\boldsymbol{i}}_S = [\underline{\boldsymbol{i}}_1, \ldots, \underline{\boldsymbol{i}}_{16}]^T$ is the (224 × 1) block vector of the entering currents in all the section. The high speed track is subjected to a current injection by the supply system: this injection occurs only at the section ends represented in Fig. 7, so the following sub-vectors are null:

$$\underline{\boldsymbol{i}}_1 \equiv \underline{\boldsymbol{i}}_4 \equiv \underline{\boldsymbol{i}}_5 \equiv \underline{\boldsymbol{i}}_8 \equiv \underline{\boldsymbol{i}}_9 \equiv \underline{\boldsymbol{i}}_{12} \equiv \underline{\boldsymbol{i}}_{13} \equiv \underline{\boldsymbol{i}}_{16} \equiv 0. \tag{10}$$

Furthermore, it could be observed that the transformer MV winding terminals are connected only at 1 ÷ 8 busbars (rails, contact wires, feeders), obviously they are not directly connected at 9 ÷ 14 busbars (messenger wire, return wires, buried ground wire); in this way, each supply section end current sub-vector $\underline{\boldsymbol{i}}_X$ has got the following arrangement:

$$\underline{\boldsymbol{i}}_X = \begin{bmatrix} \underline{\boldsymbol{i}}_X \\ \hline 0 \end{bmatrix}, \quad (X = 2, 3, 6, 7, 10, 11, 14, 15) \tag{11}$$

where $\underline{\boldsymbol{i}}_X$ is composed of eight elements. At the supply section ends only injected currents $\underline{\boldsymbol{i}}_X$ and the corresponding voltage sub-vector $\underline{\boldsymbol{u}}_{SX}$ can be considered. In (9), it can be seen that only the supplied busbars operate on the traction line, so the following relation can be written:

$$\underline{\boldsymbol{u}}_S = \underline{\boldsymbol{Z}}_S \underline{\boldsymbol{i}}_S \tag{12}$$

where the matrix $\underline{\boldsymbol{Z}}_S$ (64 × 64) can be computed starting from $\underline{\boldsymbol{Z}}_{\text{glob}}$ by means of sub-matrice (8 × 8) "extraction and recombination" method, as shown in Fig. 8.

The behavior of the supply system (composed of the three-winding transformers, the HV line and the extra-HV (EHV) grid) as seen at 1 ÷ 8 busbars of each supplied section end can be characterized by the relation

$$\underline{\boldsymbol{u}}_S = \underline{\boldsymbol{u}}_S^* - \underline{\boldsymbol{Z}}_{\text{eq}S} \underline{\boldsymbol{i}}_S \tag{13}$$

where $\underline{\boldsymbol{u}}_S^*$ is the open circuit voltage vector at supplied terminals $\underline{\text{S}}$ and $\underline{\boldsymbol{Z}}_{\text{eq}S}$ is the impedance matrix as seen at the same terminals. Obviously, this is an extension of the Thévenin theorem. The application of (12) and (13) gives

$$\underline{\boldsymbol{i}}_S = (\underline{\boldsymbol{Z}}_S + \underline{\boldsymbol{Z}}_{\text{eq}S})^{-1} \underline{\boldsymbol{u}}_S^* \tag{14}$$

which allows determining the regime of the entire system. Once the current vector $\underline{\boldsymbol{i}}_S$ is computed, by exploiting (11), it is possible to calculate each supply section end current sub-vector $\underline{\boldsymbol{i}}_X$, hence, the current vector $\underline{\boldsymbol{i}}_S$ can be substituted in (9), so, the voltage sub-vector in all the section ends are calculated and also the 9÷14 busbars voltages are known. The

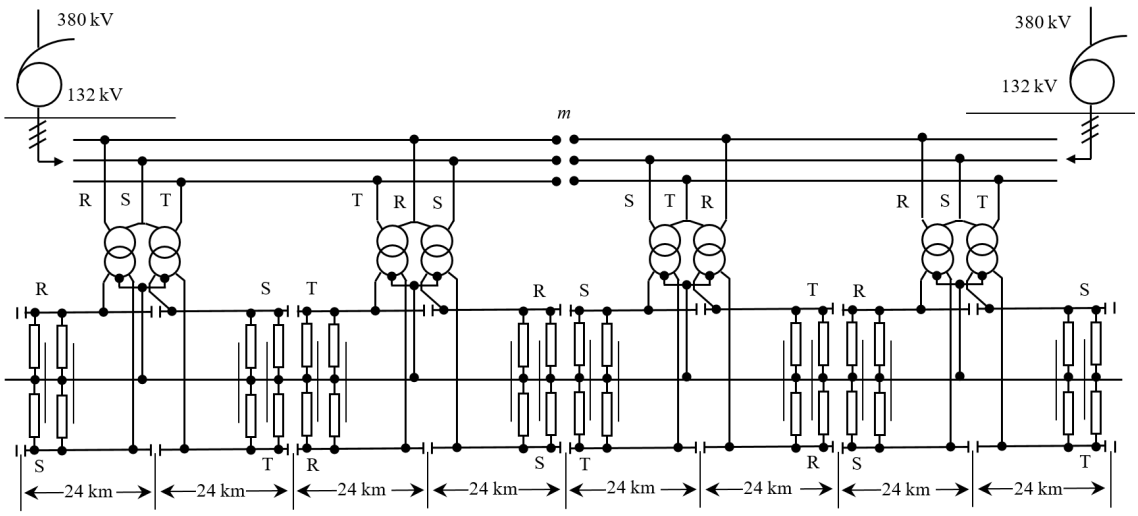

Fig. 5. AC 2 × 25 kV high-speed railway system typical configuration.

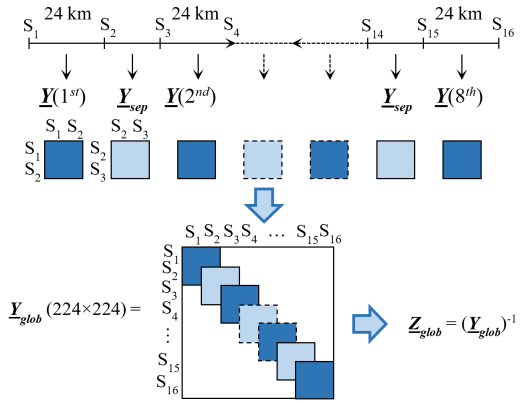

Fig. 6. Composition of the global matrix by means of section and partial-separation matrices.

knowledge of the voltage vector at the section ends represents the steady-state regime of the whole multiconductor system.

The mutual coupling between the traction line and the HV supply line can be neglected: this is possible due to the distance between the two lines and the absence of zero sequence current on the three-phase line.

V. Supply System Matrix Model

In order to combine the supply system matrix model represented in Fig. 7, the models of the elements $a_2, a_3, \ldots, d_{14}, d_{15}$ are necessary. These elements model: the connections between the transformer HV winding terminals and the HV line; the connection between the transformer MV winding terminals, the contact wires $5 \div 6$ (which are connected by the droppers, at the messenger wires $9 \div 10$), the feeders $7 \div 8$ and the rails $1 \div 4$. For instance, Fig. 9 shows the block a_2 typical configuration: the other blocks have got similar structure, the only difference is the permutation between the transformer HV terminals and the HV line. The configuration with a unique 132 kV feeder allows obtaining good behavior in terms of unbalance factor. In fact, it is possible to achieve a complete phase permutation of the transformer HV terminals by means of three two-phase drains. The easiest procedure to compute the block a_2 consists in:

1) starting from transformer plate data, it is possible to calculate the three-winding transformer equivalent admittances;
2) assembling the "primitive matrix," which models each "branch" of the block;
3) forming the incidence matrix that represents the grid topology;
4) computing the admittance matrix by exploiting the well-known formulation; and
5) removing the $a \div e$ nodes (a smarter approach can be obtained if these nodes are positioned at the end of the matrix) so the matrix $\underline{\boldsymbol{Y}}_{a2}$ (11×11) can be obtained. This matrix appears in the following equation:

$$\begin{bmatrix} \underline{\boldsymbol{i}}_{A2} \\ \underline{\boldsymbol{i}}_{S2} \end{bmatrix} = \left[\begin{array}{c|c} \underline{\boldsymbol{Y}}_{AA2} & -\underline{\boldsymbol{Y}}_{AS2} \\ \hline -\underline{\boldsymbol{Y}}_{SA2} & \underline{\boldsymbol{Y}}_{SS2} \end{array}\right] \begin{bmatrix} \underline{\boldsymbol{u}}_{A2} \\ \underline{\boldsymbol{u}}_{S2} \end{bmatrix}. \tag{15}$$

By exploiting the same approach the matrices of the other blocks (up to $\underline{\boldsymbol{Y}}_{d15}$) can be obtained, all these matrices are partitioned as $\underline{\boldsymbol{Y}}_{a2}$. These partitioned matrices, and the circuit represented in Fig. 7, give the following relations:

$$\begin{aligned} \underline{\boldsymbol{i}}_{A2} + \underline{\boldsymbol{i}}_{A3} &= \underline{\boldsymbol{i}}_{A}, \quad \underline{\boldsymbol{i}}_{B6} + \underline{\boldsymbol{i}}_{B7} = \underline{\boldsymbol{i}}_{B} \\ \underline{\boldsymbol{i}}_{C10} + \underline{\boldsymbol{i}}_{C11} &= \underline{\boldsymbol{i}}_{C}, \quad \underline{\boldsymbol{i}}_{D14} + \underline{\boldsymbol{i}}_{D15} = \underline{\boldsymbol{i}}_{D} \end{aligned} \tag{16}$$

by introducing the matrix partitioning shown in Fig. 10, the following two sets of linear equations are obtained:

$$\underline{\boldsymbol{i}}_{H} = \underline{\boldsymbol{Y}}_{HH}\underline{\boldsymbol{u}}_{H} + \underline{\boldsymbol{Y}}_{HS}\underline{\boldsymbol{u}}_{S} \tag{17}$$

$$\underline{\boldsymbol{i}}_{S} = \underline{\boldsymbol{Y}}_{SH}\underline{\boldsymbol{u}}_{H} + \underline{\boldsymbol{Y}}_{SS}\underline{\boldsymbol{u}}_{S}. \tag{18}$$

The supply network (that is subjected to unbalanced currents at the busbars R, S, T of each supply section $A \div D$) is treated as a multiconductor system, which is characterized by the phase matrix $\underline{\boldsymbol{Y}}_{N}$ (12×12) as seen at the same sections. The HV supply lines are also modeled by means of MCA approach. By exploiting this approach, it is possible to avoid

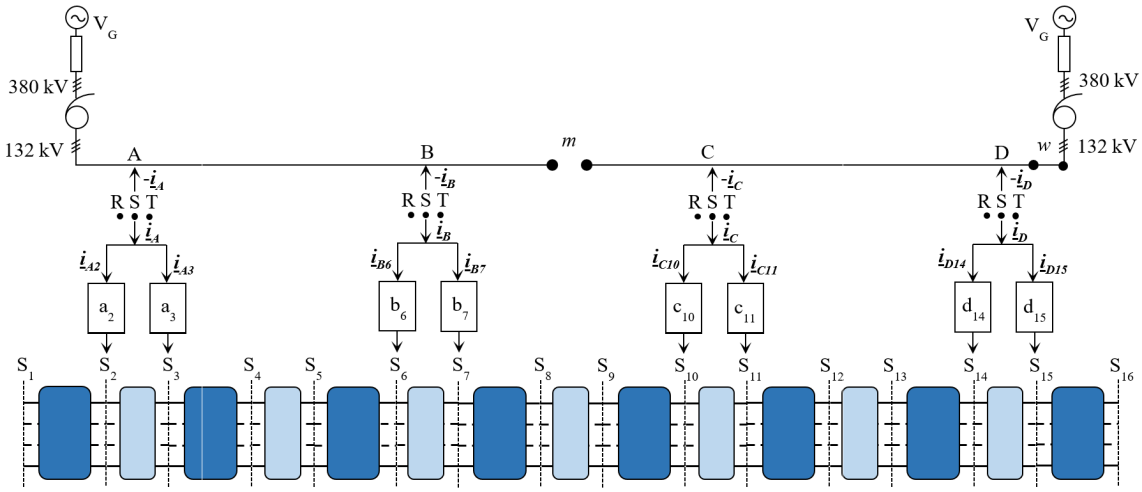

Fig. 7. Representation of the section and partial-separation matrices cascade of the AC 2 × 25 kV high-speed railway system.

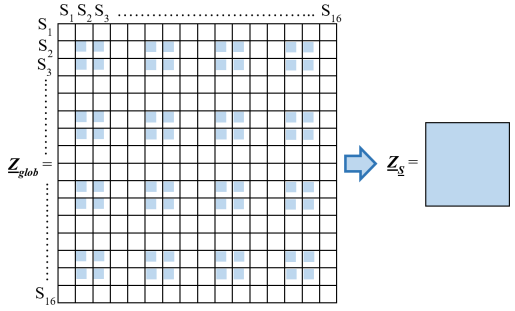

Fig. 8. Reduction of $\underline{\boldsymbol{Z}}_{\text{glob}}$ by means of the "extraction and recombination" method.

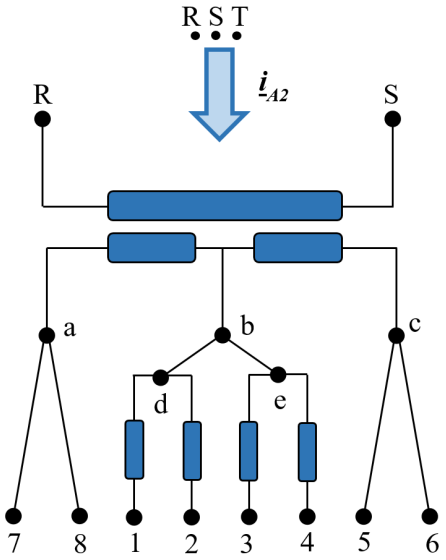

Fig. 9. Circuit model of the transformer supplying the railway line.

the sequence frame of reference approach. For the network $\boldsymbol{N}$, the injection of the vector $-\underline{\boldsymbol{i}}_H$ in the H $(A \div D)$ sections gives the following relation:

$$-\underline{\boldsymbol{i}}_H = \underline{\boldsymbol{Y}}_N \underline{\boldsymbol{u}}_H. \tag{19}$$

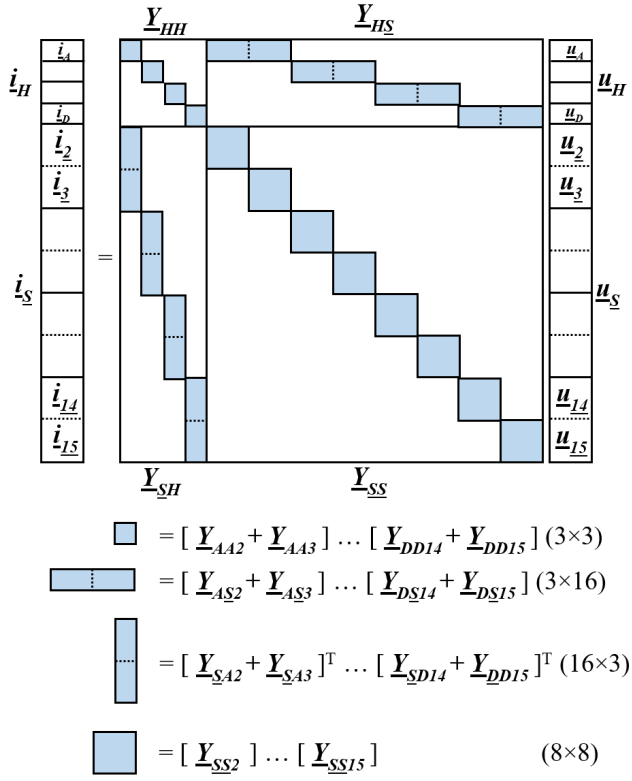

Fig. 10. Making of the admittance matrix modeling all the railway sections by means of block matrix composition.

By summing (17) and (19), member to member, the following relation yields:

$$0 = (\underline{\boldsymbol{Y}}_N + \underline{\boldsymbol{Y}}_{HH})\underline{\boldsymbol{u}}_H + \underline{\boldsymbol{Y}}_{HS}\underline{\boldsymbol{u}}_S. \tag{20}$$

From (20) it follows that:

$$\underline{\boldsymbol{u}}_H = -(\underline{\boldsymbol{Y}}_N + \underline{\boldsymbol{Y}}_{HH})^{-1}\underline{\boldsymbol{Y}}_{HS}\underline{\boldsymbol{u}}_S. \tag{21}$$

By introducing (21) in (18), i.e.,

$$\underline{\boldsymbol{i}}_S = [-\underline{\boldsymbol{Y}}_{SH}(\underline{\boldsymbol{Y}}_N + \underline{\boldsymbol{Y}}_{HH})^{-1}\underline{\boldsymbol{Y}}_{HS} + \underline{\boldsymbol{Y}}_{SS}]\underline{\boldsymbol{u}}_S. \tag{22}$$

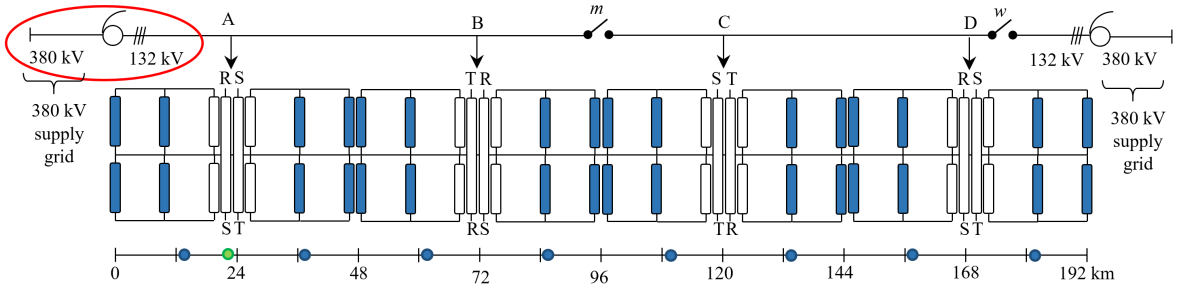

Fig. 11. Division of the railways in eight sections: the blue points represent couples of trains traveling in opposite directions, whereas the green point represents the short-circuit position.

This equation shows how the matrix $\underline{\boldsymbol{Z}}_{\text{eq}\underline{S}}$ of (13) and (14) can be computed, so that

$$\underline{\boldsymbol{Z}}_{\text{eq}\underline{S}} = [-\underline{\boldsymbol{Y}}_{\underline{S}H}(\boldsymbol{Y}_N + \underline{\boldsymbol{Y}}_{HH})^{-1}\underline{\boldsymbol{Y}}_{H\underline{S}} + \underline{\boldsymbol{Y}}_{\underline{SS}}]^{-1}. \tag{23}$$

The supply network matrix $\underline{\boldsymbol{Y}}_N$ (12 × 12) has got different compositions due to the network layout. For instance, in Fig. 7 the "nominal" configuration is shown (with the breaker m open), however, in emergency situations the grid could present a different structure (with the breaker m close and w open). The assessment of the sub-vector $\underline{\boldsymbol{u}}^*_{\underline{S}}$, in phase and magnitude, can be easily obtained. These elements depend on the line to line voltages taken from the blocks $a_2, a_3, \ldots, d_{14}, d_{15}$.

VI. Case Studies

In order to demonstrate the strength of the MCA algorithm applied to the study of the AC high speed railway lines, two different scenarios are considered: a high load scenario and a faulty one. The present approach is implemented in a MATLAB environment. The analyses must be considered as a snapshot assessment of the electrical quantities occurring along the railway track.

The analyzed railway is 192 km long. The railway is divided into sections, subsections, and elementary cells as follows.

1) Eight sections, each one 24 km long.
2) Thirty-two subsections in each section. Each subsection is 750 m long.
3) Twelve elementary cells in each subsection. Each elementary cell is 62.5 m long.

The earth resistivity is set to 100 Ωm. The correctness of this value is fundamental in order to make accurate evaluations of the ground return currents. An accurate ground return current assessment, in fact, allows making precise evaluations of EMIs on parallel conductors (e.g., telecommunications, gas, etc.).

With regard to the network supplying the 2 × 25 kV contact wire system, there are:

1) an upstream 380 kV EHV supply network characterized by the following values of short circuit currents: $I_{\text{sc}3p} = 20$ kA, $I_{\text{sc}1p} = 16.4$ kA (the three-phase short-circuit power is equal to 13.2 GVA);
2) two three-phase 380/132 kV auto-transformers feeding the 132 kV HV supply network; and
3) eight two-phase 132/25 kV transformers.

The evaluations in the following simulations are performed in terms of:

1) voltage trends on the contact wire;
2) current trends on both the contact wire and in the ground; and
3) voltage unbalance factors in the three-phase grid feeding the railway system (percentual ratio between the negative sequence voltage and the sequence positive one [28]).

Differently from the algorithms developed so far [4], [5], [6], [7], [8], [9], [10], [11], [12], in this MCA algorithm no simplifying hypothesis is assumed, and very accurate evaluations can be performed (see Section I-A).

A. Maximum Allowable High-Speed Line Power Request

This scenario considers the simultaneous presence of 16 trains in the entire railway track. The trains are grouped into eight pairs. The trains of each pair travel in opposite directions and are split on the two rails. The distance of each pair of trains is 24 km, which means that the trains travel at a speed of 300 km/h (being in a 5 min interval).

It is supposed that the railway system is supplied only by the left 380/132 kV auto-transformer (see red circle in Fig. 11). In fact, the breaker m is closed, whereas the breaker w is open (see Fig. 7).

In Fig. 11 the blue points represent the positioning of all the train pairs inside the entire railway track. Each pair of trains is supposed to be in the 20$^{\text{th}}$ subsection of each section. Each train absorbs a power equal to 9.8 MW.

Fig. 12 represents both the voltage and the ground return current trends over the railway distance thoroughly. The gray curve represents the root mean square (rms) voltage of the contact wire. The black curve represents the ground return current along the distance. It is worth observing that the voltage trend is nearly constant in each section: the lowest voltage value is in the eighth section. This value can be adjusted by means of on load tap changer transformers (OLTCs).

The voltage unbalance factors [**UF**s (%)] of the AC high-speed railway supply system are computed in 132 kV A–D nodes, and in the 380 kV delivery node (see Fig. 11) and shown in Table I.

Fig. 13 represents the voltage unbalance factor trend as a function of the three-phase short circuit current in the 380 kV

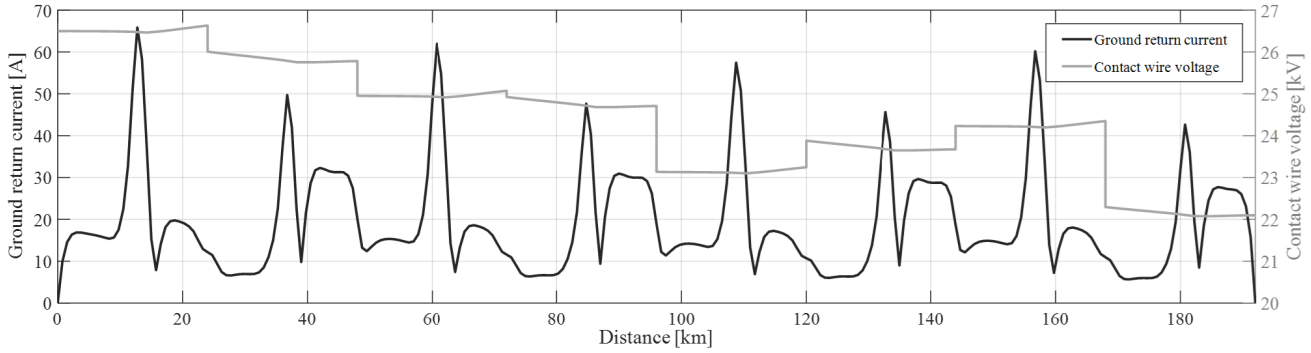

Fig. 12. Ground current and wire contact voltage trend over the railway distance.

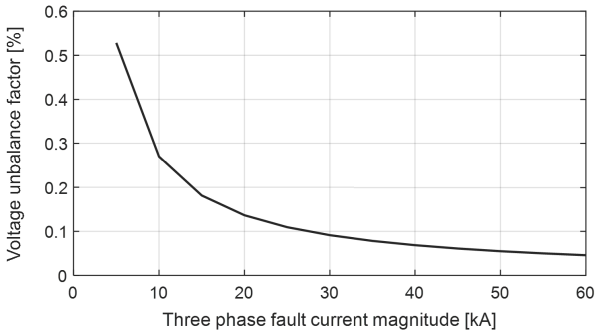

Fig. 13. Voltage unbalance factor trend as a function of the three-phase current value.

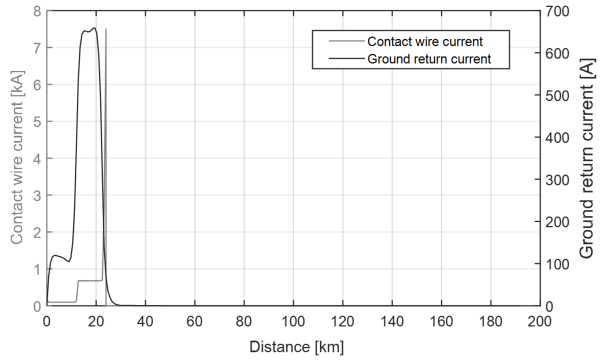

Fig. 14. Contact wire current and ground return current over the railway distance.

TABLE I

UNBALANCE FACTORS IN POINTS: 380 kV DELIVERY NODE, A–D OF THE FEEDER SYSTEM

	380 kV delivery node	132 kV A node	132 kV B node	132 kV C node	132 kV D node
UF [%]	0.14	1.57	1.70	2.95	5.17

TABLE II

UNBALANCE FACTORS IN POINTS A–D OF THE FEEDER SYSTEM AND ON THE TWO 380 kV NODES REPRESENTED IN FIG. 11

	Left 380 kV delivery node	Right 380 kV delivery node	132 kV A node
UF [%]	1.78	0.001	24.85
	132 kV B node	132 kV C node	132 kV D node
UF [%]	24.80	0.006	0.006

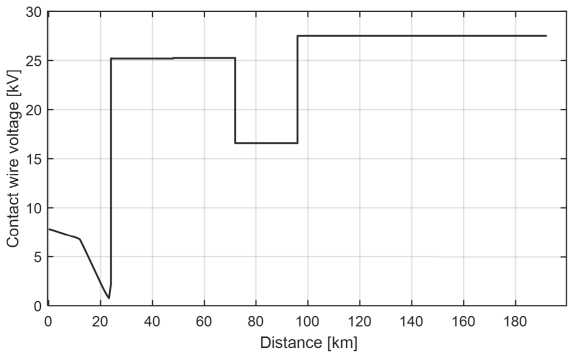

Fig. 15. Contact wire (conductor 5) voltage trend along the railway distance.

delivery node. Certainly, the positioning of the train is kept constant for each different short-circuit current evaluation.

The simulations are performed by varying the three-phase current value in the range $(5 \div 60)$ kA, and the single-phase current one in the range $(3.8 \div 50)$ kA. Thus, 12 equidistant pairs of values are extracted from these two ranges (equidistant variations of 5 and 4.2 kA for the three-phase and single-phase currents, respectively).

B. Fault in k Position

A faulty regime study due to a short-circuit occurring between the contact wire and the rails is performed. The involved short-circuit conductors are the contact wire 5 and the rails $1 \div 2$. The green point in Fig. 11 is the fault position occurring in the 32nd subsection of the first section. This section is the closest to the power supply and it is chosen to have a conservative evaluation: the closer is the fault point, the higher the short-circuit currents. In this case, the 132 kV feeder is operated with the *m* breaker open, so supplied by both 380 kV nodes. It is not considered the presence of trains in the railway, according to the IEC 60909-0 [29].

Fig. 14 represents the ground return current and contact wire current trends in faulty regime along the railway positioning.

Fig. 15 shows the rms voltage trend in this faulty regime as a function of the railway distance. It is worth noting that the fourth section $(72 \div 96$ km) suffers of a voltage dip

(the magnitude is equal to 18 kV), since it is the section supplied by the HV line to line voltage RS (the same feeding the faulty section). Table II represents the voltage unbalance factors of the railway supply system in nodes A–D, and in the two 380 kV delivery nodes feeding the entire railway supply system (see Fig. 11). These values are easily obtained by means of MCA once the symmetrical components are derived from the phase frame of reference.

VII. Conclusion

A novel MCA application studying both the 2 × 25 kV AC high-speed railway system and the three-phase upstream HV supply network is presented. The MCA matrix approach allows making a detailed assessment of all the electrical quantities along the railway track. The interactions between the railway lines and the upstream HV supply network, and the EMIs on parallel metal conductors can be assessed. This evaluation is possible by the knowledge of the ground return current, which is an outcome of the algorithm.

The procedure is totally general since it can investigate various scenarios (nominal, high/low power absorptions, faulty, etc.), for different system geometrical configurations, and for any number of trains/conductors. Nowadays, no existing open algorithm or closed software allows assessing all the electrical quantities for the high-speed railways in a detailed manner compared to MCA. The method is completely open and it can be self-implemented in any Math-packages by using any scripting language (i.e., MATLAB, Python, etc.).

Several simulations have been performed and two of these are fully presented in the article: the former represents a high power absorption scenario, and the latter deals with a faulty occurrence. In both scenarios, the unbalance factors are evaluated presenting high values (up to 24%) in case of contact-wire-to-rail short circuit. The behavior of the ground return current and the contact wire voltage is presented for the high load scenario, with maximum ground return current magnitude of about 70 A and contact wire voltage drop of about 12%.

Further research studies are on-going toward the integration of such procedures in the three-phase power flow in order to assess the unbalance power absorption due to the high-speed railway system.

References

[1] *Fostering the Railway Sector Through the European Green Deal*, European Union Agency for Railways, Valenciennes, France, 2020, p. 4.

[2] *Sustainable and Smart Mobility Strategy Putting European Transport on Track for the Future*, European Commission, Brussels, Belgium, 2020, pp. 2–3.

[3] *The Future of Rail*, IEA, Paris, France, Jan. 2019, p. 48.

[4] E. Pilo, L. Rouco, and A. Fernandez, "A reduced representation of 2×25 kV electrical systems for high-speed railways," in *Proc. IEEE/ASME Joint Railroad Conf.*, Apr. 2003, pp. 199–205.

[5] E. Pilo, L. Rouco, A. Fernandez, and A. Hernández-Velilla, "A simulation tool for the design of the electrical supply system of high-speed railway lines," in *Proc. IEEE Power Eng. Soc. Summer Meeting*, Jul. 2000, vol. 2, pp. 1053–1058.

[6] I. Bodnar and G. Varju, "Effect of the intervals between the bonds of overhead line and reinforcing feeder wire in the case of 25 kV traction feeding at 50 Hz," in *Proc. 4th Int. Youth Conf. Energy (IYCE)*, Jun. 2013, pp. 1–6.

[7] M. Plakhova, B. Mohamed, and P. Arboleya, "Graph theory approach for a 2×25kV AC bivoltage traction system," in *Proc. 6th Int. Conf. Power Electron. Syst. Appl. (PESA)*, Dec. 2015, pp. 1–5.

[8] X. He, Y. Wen, and D. Zhang, "Influence of protection wire and positive feeder arrangement of traction network on the return current in high-speed railway," in *Proc. IEEE 2nd Int. Conf. Electron. Technol., Commun. Inf. (ICETCI)*, May 2022, pp. 205–210.

[9] R. Cella et al., "Measurement of AT electric railway system currents at power-supply frequency and validation of a multiconductor transmission-line model," *IEEE Trans. Power Del.*, vol. 21, no. 3, pp. 1721–1726, Jul. 2006.

[10] W. Mingli, C. Roberts, and S. Hillmansen, "Modelling of AC feeding systems of electric railways based on a uniform multi-conductor chain circuit topology," in *Proc. IET Conf. Railway Traction Syst. (RTS)*, 2010, pp. 1–5.

[11] M. Brenna and F. Foiadelli, "Sensitivity analysis of the constructive parameters for the 2 × 25-kV high-speed railway lines planning," *IEEE Trans. Power Del.*, vol. 25, no. 3, pp. 1923–1931, Jul. 2010.

[12] J. D. Glover, A. Kusko, and S. M. Peeran, "Train voltage analysis for AC railroad electrification," *IEEE Trans. Ind. Appl.*, vol. IA-20, no. 4, pp. 925–934, Jul. 1984.

[13] A. Mariscotti, P. Pozzobon, and M. Vanti, "Distribution of the traction return current in AT electric railway systems," *IEEE Trans. Power Del.*, vol. 20, no. 3, pp. 2119–2128, Jul. 2005.

[14] A. Dolara, M. Gualdoni, and S. Leva, "Impact of high-voltage primary supply lines in the 2 × 25 kV–50 Hz railway system on the equivalent impedance at pantograph terminals," *IEEE Trans. Power Del.*, vol. 27, no. 1, pp. 164–175, Jan. 2012.

[15] R. Benato and R. Caldon, "Distribution line carrier: Analysis procedure and applications to DG," *IEEE Trans. Power Del.*, vol. 22, no. 1, pp. 575–583, Jan. 2007.

[16] R. Benato and A. Paolucci, "Multiconductor cell analysis of skin effect in Milliken type cables," *Electr. Power Syst. Res.*, vol. 90, pp. 99–106, Sep. 2012.

[17] R. Benato and S. D. Sessa, "A new multiconductor cell three-dimension matrix-based analysis applied to a three-core armoured cable," *IEEE Trans. Power Del.*, vol. 33, no. 4, pp. 1636–1646, Aug. 2018.

[18] R. Benato, S. D. Sessa, M. Forzan, M. Poli, F. Sanniti, and R. Torchio, "HVAC single core insulated cables with steel reinforced mechanical protections: Effect on sequence impedances," *IEEE Trans. Power Del.*, vol. 36, no. 3, pp. 1663–1671, Jun. 2021.

[19] R. Benato, S. D. Sessa, M. Poli, and F. Sanniti, "Sequence impedances of land single-core insulated cables: Direct formulae and multiconductor cell analyses compared with measurements," *Energies*, vol. 13, no. 5, p. 1084, Mar. 2020.

[20] R. Benato, S. D. Sessa, and M. Forzan, "Experimental validation of three-dimension multiconductor cell analysis by a 30 km submarine three-core armoured cable," *IEEE Trans. Power Del.*, vol. 33, no. 6, pp. 2910–2919, Dec. 2018.

[21] R. Benato, S. D. Sessa, G. Gardan, F. Palone, and F. Sanniti, "Experimental harmonic validation of 3D multiconductor cell analysis: Measurements on the 100 km long sicily-malta 220 kV three-core armoured cable," *IEEE Trans. Power Del.*, vol. 37, no. 1, pp. 573–581, Feb. 2022.

[22] W. Mingli, C. Roberts, and S. Hillmansen, "Modelling of AC feeding systems of electric railways based on a uniform multi-conductor chain circuit topology," in *Proc. IET Conf. Railway Traction Syst. (RTS)*, 2010, pp. 1–5.

[23] H. Lee, C. Lee, G. Jang, and S.-H. Kwon, "Harmonic analysis of the Korean high-speed railway using the eight-port representation model," *IEEE Trans. Power Del.*, vol. 21, no. 2, pp. 979–986, Apr. 2006.

[24] R. Benato, S. D. Sessa, and F. Guglielmi, "Determination of steady-state and faulty regimes of overhead lines by means of multiconductor cell analysis (MCA)," *Energies*, vol. 5, no. 8, pp. 2771–2793, Jul. 2012.

[25] R. Benato, "Multiconductor analysis of underground power transmission systems: EHV AC cables," *Electr. Power Syst. Res.*, vol. 79, no. 1, pp. 27–38, Jan. 2009.

[26] G. W. Stagg and A. H. El-Abiad, *Computer Methods in Power System Analysis*. New York, NY, USA: McGraw-Hill, 1968.

[27] R. Benato, "Advanced matrix technique for dynamic and steady state evaluation of power systems," Ph.D. dissertation, Dept. Elect. Eng., Padova Univ., Padova, Italy, 1998.

[28] R. Benato, G. Gardan, and L. Rusalen, "A three-phase power flow algorithm for transmission networks: A hybrid phase/sequence approach," *IEEE Access*, vol. 9, pp. 162633–162650, 2021.

[29] *Short-Circuit Currents in Three-Phase A.C. Systems. Calculation of Currents*, document IEC 60909-0, 2001.

Roberto Benato (Senior Member, IEEE) was born in Venice, Italy, in 1970. He received the Dr.Ing. degree in electrical engineering from the University of Padua, Padua, Italy, in 1995, and the Ph.D. degree in power systems analysis from the University of Padua in 1999.

In 2011, he was appointed as an Associate Professor with the Department of Industrial Engineering, University of Padua. He is the author of 220 articles and five books, edited by Springer, Wolters Kluwer, and China Machine Press.

Dr. Benato has been a member of six Cigré Working Groups (WGs) and the Secretary of two Joint WGs, and a member of the IEEE Power & Energy Society Substations Committee. In 2014, he was nominated as a member of the IEC TC 120 "Electrical Energy Storage (EES) Systems" in the WG 4 "Environmental Issues of EES Systems." Currently, he is a Corresponding Member of Cigré WG B1.72 "Cable Rating Verification Second Part." In 2018, he was elevated to the grade of a Cigré Distinguished Member. He is also a member of The Italian Association of Electrical, Electronics, Automation, Informatics and Telecomunications (AEIT).

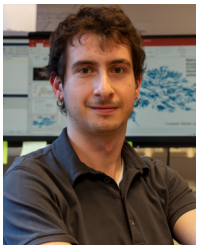

Giovanni Gardan (Member, IEEE) was born in Venice, Italy, in 1995. He received the B.S. degree in energy engineering and the Dr.Ing. degree in electrical engineering from the University of Padua, Padua, Italy, in 2017 and 2020, respectively, where he is currently pursuing the Ph.D. degree in industrial engineering.

His main fields of research are electrical energy transmission and power systems computation.

Dr. Gardan is a Young Member of Cigré and The Italian Association of Electrical, Electronics, Automation, Informatics and Telecomunications (AEIT).

Luca Rusalen (Member, IEEE) was born in Treviso, Italy, in 1996. He received the bachelor's degree in energy engineering and the Dr.-Ing. degree in electrical engineering from the University of Padua, Padua, Italy, in 2019 and 2021, respectively, where he is currently pursuing the Ph.D. degree in industrial engineering.

His research interests include computer analysis of power systems and transmission line modeling.

Dr. Rusalen is a Young Member of The Italian Association of Electrical, Electronics, Automation, Informatics and Telecomunications (AEIT).

Open Access funding provided by 'Università degli Studi di Padova' within the CRUI CARE Agreement